Theory of magnetic switching of ferroelectricity in spiral magnets

Masahito Mochizuki[1] and Nobuo Furukawa[2, 3]

[1]*Department of Applied Physics, University of Tokyo, Tokyo 113-8656, Japan*
[2]*Department of Physics, Aoyama Gakuin University, Sagamihara, 229-8558 Japan*
[3]*Multiferroics Project, ERATO, Japan Science and Technology Agency (JST), Tokyo 113-8656, Japan*

We propose a microscopic theory for magnetic switching of electric polarization ($\boldsymbol{P}$) in the spin-spiral multiferroics by taking $TbMnO_3$ and $DyMnO_3$ as examples. We reproduce their phase diagrams under a magnetic field $\boldsymbol{H}_{\rm ex}$ by Monte-Carlo simulation of an accurate spin model and reveal that competition among the Dzyaloshinskii-Moriya interaction, spin anisotropy, and spin exchange is controlled by the applied $\boldsymbol{H}_{\rm ex}$, resulting in magnetic transitions accompanied by reorientation or vanishing of $\boldsymbol{P}$. We also discuss the relevance of the proposed mechanisms to many other multiferroics such as $LiCu_2O_2$, $MnWO_4$, and $Ni_3V_2O_4$.

PACS numbers: 77.80.Fm, 75.80.+q, 75.30.Gw, 75.47.Lx

Concurrently magnetic and ferroelectric materials, i.e. multiferroics, offer prospective systems to attain magnetic control of electricity via magnetoelectric (ME) coupling [1, 2]. It was experimentally demonstrated that an external magnetic field ($\boldsymbol{H}_{\rm ex}$) can cause reorientation, emergence, and vanishing of ferroelectric polarization $\boldsymbol{P}$ in many spin-spiral multiferroics such as RMnO$_3$ (R=Tb, Dy, $Eu_{1-x}Y_x$, etc) [3–5], $LiCu_2O_2$ [6], $MnWO_4$ [7], and $Ni_3V_2O_4$ [8]. These ME phenomena are currently attracting enormous interest, and a thorough understanding of their mechanisms is an urgent issue. However, the number of theoretical studies is very few despite many experimental reports. Naively, the applied $\boldsymbol{H}_{\rm ex}$ can determine the direction of $\boldsymbol{P}$ by controlling the conical spin structure via Zeeman coupling, but there are many examples that do not obey this simple picture.

In the spin-spiral multiferroics, inherent spin frustration as an origin of the spiral magnetism inevitably reduces the spin-exchange energy, and hence increases the relative importance of other tiny interactions, e.g. the single-ion spin anisotropy and the Dzyaloshinskii-Moriya (DM) interaction. Consequently, the magnetic switching of $\boldsymbol{P}$ in this new class of multiferroics is governed by their fine energy balance tuned by $\boldsymbol{H}_{\rm ex}$, which cannot be understood from a simple interplay between Zeeman coupling and the spin exchanges.

In this Letter, by taking the Mn perovskites $TbMnO_3$ and $DyMnO_3$ as examples, we propose a microscopic theory for the magnetic control of $\boldsymbol{P}$ in the spin-spiral multiferroics. Their puzzling T-$H_{\rm ex}$ phase diagrams are reproduced by the Monte-Carlo (MC) analysis of an accurate spin model. Our microscopic theory reveals that the applied $\boldsymbol{H}_{\rm ex}$ controls conflicts among the spin exchanges, spin anisotropy, and DM interaction, resulting in magnetic transitions accompanied by reorientation or vanishing of $\boldsymbol{P}$. The mechanisms proposed here are relevant to many other spin-spiral multiferroics such as $LiCu_2O_2$ [6], $MnWO_4$ [7], and $Ni_3V_2O_4$ [8]. We also discuss the influence of effective magnetic fields from rare-earth f moments.

The ferroelectricity in these materials is described by the spin-current model [9, 10] as given by $\boldsymbol{P} \propto \boldsymbol{Q} \times \boldsymbol{\chi}$, where $\boldsymbol{Q}$ is a propagation vector of the spiral and $\boldsymbol{\chi} \propto \sum_{<i,j>} \boldsymbol{S}_i \times \boldsymbol{S}_j$ is the vector spin chirality. As shown in Fig 1(b), the Mn spins in $TbMnO_3$ and $DyMnO_3$ are rotating within the bc plane ($\boldsymbol{\chi} \| \boldsymbol{a}$) to form a transverse spiral with $\boldsymbol{Q} \| \boldsymbol{b}$ [11], and thus $\boldsymbol{P} \| \boldsymbol{c}$ is realized.

In Figs. 1(c)-(f), we briefly summarize the puzzles in RMnO$_3$ [4]. The applied $\boldsymbol{H}_{\rm ex}$ induces the magnetization $\boldsymbol{M} \| \boldsymbol{H}_{\rm ex}$ via Zeeman coupling, and hence forces the spin structure to be conical where $\boldsymbol{\chi} \| \boldsymbol{H}_{\rm ex}$. When we apply $\boldsymbol{H}_{\rm ex} \| \boldsymbol{Q}$ [see Fig. 1(c)], we expect a longitudinal conical spin order with $\boldsymbol{\chi} \| \boldsymbol{Q}$. In this case, $\boldsymbol{P}$ should be zero within the spin-current model. Thus we expect vanishing of $\boldsymbol{P}$ when we apply $\boldsymbol{H}_{\rm ex} \| \boldsymbol{b}$ (*Pbnm* setting) to $TbMnO_3$ and $DyMnO_3$. However, reorientation of $\boldsymbol{P}$ from $\boldsymbol{P} \| \boldsymbol{c}$ to $\boldsymbol{P} \| \boldsymbol{a}$ is observed in reality [see Fig. 1(e)]. A neutron-scattering experiment confirmed that this $\boldsymbol{P}$ reorientation results from the spin-chirality flop from $\boldsymbol{\chi} \| \boldsymbol{a}$ to $\boldsymbol{\chi} \| \boldsymbol{c}$ [12, 13]. This discrepancy has been naively attributed to the influence of f moments on the rare-earth ions thus far [15, 16]. However, a similar behavior has been observed also in $LiCu_2O_2$ without f moments [6], suggesting an essentially new mechanism. Mostovoy reproduced the flop by introducing higher-order anisotropies in a *phenomenological* theory although their microscopic origins are unclear [9]. On the other hand, the application of $\boldsymbol{H}_{\rm ex} \perp \boldsymbol{Q}$ is expected to stabilize a transverse conical spin order with $\boldsymbol{\chi} \perp \boldsymbol{Q}$. As shown in Fig. 1(d), we expect the ab-plane transverse conical order with $\boldsymbol{P} \| \boldsymbol{a}$ when we apply $\boldsymbol{H}_{\rm ex} \| \boldsymbol{c}$ to $TbMnO_3$ and $DyMnO_3$. However, in $TbMnO_3$, the first-order transition to paraelectric ($\boldsymbol{P}$=0) phase is observed under $\boldsymbol{H}_{\rm ex} \| \boldsymbol{c}$ as shown in Fig. 1(f). The $\boldsymbol{H}_{\rm ex}$-induced vanishing of $\boldsymbol{P}$ is also observed in $MnWO_4$ [7] and $Ni_3V_2O_4$ [8].

To solve these puzzles, we start with a classical Heisenberg model on a cubic lattice, in which the Mn S=2 spins are treated as classical vectors. The Hamiltonian is given by $\mathcal{H} = \mathcal{H}_J + \mathcal{H}_{\rm sia} + \mathcal{H}_{\rm DM} + \mathcal{H}_{\rm Zeeman}$. The first term $\mathcal{H}_J = \sum_{<i,j>} J_{ij} \boldsymbol{S}_i \cdot \boldsymbol{S}_j$ describes spin-exchange in-

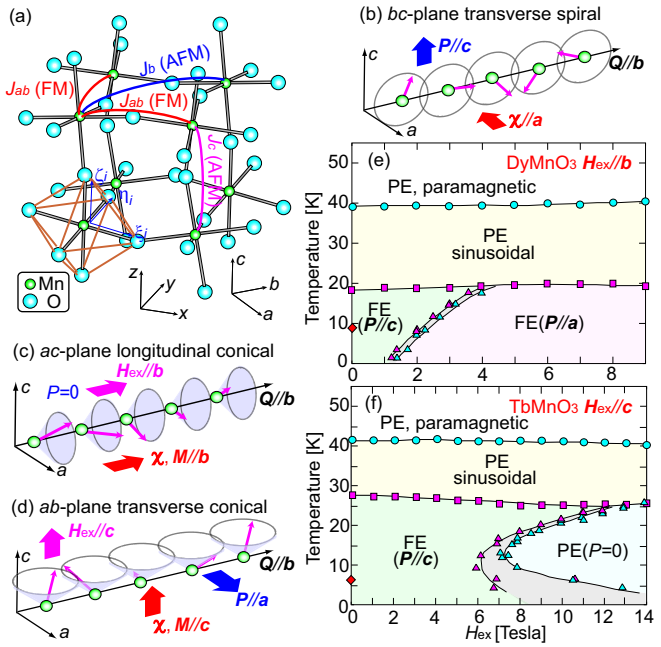

FIG. 1: (color online). (a) Crystal structure, spin exchanges, and local axes ξ_i, η_i, and ζ_i in RMnO$_3$. Here FM (AFM) denotes (anti)ferromagnetic exchange. (b) bc-plane transverse spin spiral in TbMnO$_3$ and DyMnO$_3$, which induces ferroelectric polarization $\boldsymbol{P}\|\boldsymbol{c}$. (c) [(d)] Application of $\boldsymbol{H}_{\rm ex}\|\boldsymbol{b}$ [$\boldsymbol{H}_{\rm ex}\|\boldsymbol{c}$] is expected to stabilize the longitudinal [transverse] spin spiral with magnetization $\boldsymbol{M}\|\boldsymbol{H}_{\rm ex}$ where $\boldsymbol{P}$=0 [$\boldsymbol{P}\|\boldsymbol{a}$] is expected within the spin-current model. (e)[(f)] Experimental T-$H_{\rm ex}$ phase diagram of DyMnO$_3$ [TbMnO$_3$] for $\boldsymbol{H}_{\rm ex}\|\boldsymbol{b}$ [$\boldsymbol{H}_{\rm ex}\|\boldsymbol{c}$] from Ref. [4], which shows reorientation of $\boldsymbol{P}$ from $\boldsymbol{P}\|\boldsymbol{c}$ to $\boldsymbol{P}\|\boldsymbol{a}$ [disappearance of $\boldsymbol{P}$] [4]. Here FE (PE) denotes ferroelectric (paraelectric) phase.

teractions as shown in Fig. 1(a). The second term $\mathcal{H}_{\rm sia}$ denotes the single-ion spin anisotropy, which consists of two parts as $\mathcal{H}_{\rm sia}=\mathcal{H}^D_{\rm sia}+\mathcal{H}^E_{\rm sia}$ with $\mathcal{H}^D_{\rm sia}=D\sum_i S^2_{\zeta i}$ and $\mathcal{H}^E_{\rm sia}=E\sum_i(-1)^{i_x+i_y}(S^2_{\xi i}-S^2_{\eta i})$. Here ξ_i, η_i and ζ_i are the tilted local axes attached to the ith MnO$_6$ octahedron [17]. The term $\mathcal{H}^D_{\rm sia}$ causes the hard-axis anisotropy along $\boldsymbol{c}$, or, equivalently, the easy-plane anisotropy in the ab plane. The third term $\mathcal{H}_{\rm DM}=\sum_{<i,j>}\boldsymbol{d}_{i,j}\cdot(\boldsymbol{S}_i\times\boldsymbol{S}_j)$ represents the DM interaction where the vectors $\boldsymbol{d}_{i,j}$ are defined on the Mn(i)-O-Mn(j) bonds, and are expressed by five DM parameters, α_{ab}, β_{ab}, γ_{ab}, α_c, and β_c [18]. This term consists of two parts, $\mathcal{H}^{ab}_{\rm DM}$ and $\mathcal{H}^{c}_{\rm DM}$, where $\mathcal{H}^{ab}_{\rm DM}$ ($\mathcal{H}^{c}_{\rm DM}$) is associated with the DM vectors on the in-plane (out-of-plane) Mn-O-Mn bonds. The last term, $\mathcal{H}_{\rm Zeeman}=g\mu_{\rm B}\sum_i\boldsymbol{S}_i\cdot\boldsymbol{H}_{\rm in}$, stands for the Zeeman coupling. Note that the Mn spins feel the internal magnetic field $\boldsymbol{H}_{\rm in}$, which consists of two contributions, i.e., the applied field $\boldsymbol{H}_{\rm ex}$ and the effective field $\boldsymbol{H}_{fd}$ from the f moments. This model has successfully reproduced the phase diagrams of RMnO$_3$ at $\boldsymbol{H}_{\rm ex}$=0 [19].

We have microscopically determined the values of J_{ab}, J_b, J_c, D, and E, and have estimated the values of five

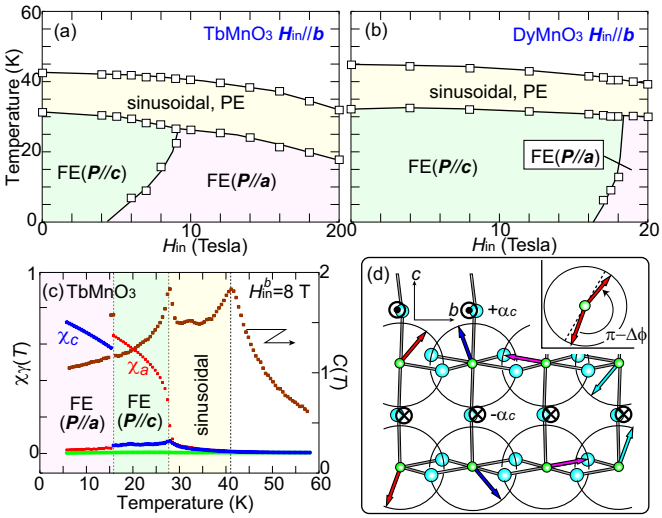

FIG. 2: (color online). Theoretical T-$H_{\rm in}$ phase diagrams of (a) TbMnO$_3$ and (b) DyMnO$_3$ for $\boldsymbol{H}_{\rm in}\|\boldsymbol{b}$. (c) T profiles of specific heat $C(T)$ and spin chiralities $\chi_\gamma(T)$ (γ=a, b, c) for TbMnO$_3$ at $H^b_{\rm in}$=8 T. (d) Spin structure in the bc-plane spiral state at $H_{\rm in}$=0, and arrangement of the a-axis components of DM vectors on the out-of-plane Mn-O-Mn bonds. The symbols $\odot$ and $\otimes$ express their signs, i.e., positive and negative, respectively. In the inset, the arrows (dashed lines) show the spin directions in the presence (absence) of DM interaction.

DM parameters in Ref. [19]. We perform calculations using two sets of the model parameters (A and B) as (A) (J_{ab}, J_b, J_c)=(−0.74, 0.64, 1.0), (D, E)=(0.2, 0.25), (α_{ab}, β_{ab}, γ_{ab})=(0.1, 0.1, 0.14) and (α_c, β_c)=(0.48, 0.1), and (B) (J_{ab}, J_b, J_c)=(−0.7, 0.99, 1.0), (D, E)=(0.22, 0.25), (α_{ab}, β_{ab}, γ_{ab})=(0.1, 0.1, 0.14) and (α_c, β_c)=(0.45, 0.1). Here the energy unit is meV. These parameter sets give the bc-plane spin spirals propagating along the b axis with wave numbers Q_b=0.3π and Q_b=0.4π, respectively. They reproduce well the spiral spin states in TbMnO$_3$ (Q_b=0.28π) [11] and DyMnO$_3$ (Q_b=0.39π) [4] at $H_{\rm ex}$=0.

We analyze this model using the replica-exchange MC technique [20]. Each exchange sampling is taken after 400 standard MC steps. After 600 exchanges for thermalization, we typically perform 1000 exchanges for systems of N=40×40×6 sites with periodic boundaries.

In Figs. 2(a) and (b) we display theoretically obtained T-$H_{\rm in}$ phase diagrams of TbMnO$_3$ and DyMnO$_3$ for $\boldsymbol{H}_{\rm in}\|\boldsymbol{b}$, respectively. They successfully reproduce the observed reorientation of $\boldsymbol{P}$ from $\boldsymbol{P}\|\boldsymbol{c}$ to $\boldsymbol{P}\|\boldsymbol{a}$ as a flop of the spin chirality from $\boldsymbol{\chi}\|\boldsymbol{a}$ to $\boldsymbol{\chi}\|\boldsymbol{c}$. We determine the transition points and the spin structures by calculating the T dependence of specific heat $C(T)=\frac{1}{N}\partial\langle\mathcal{H}\rangle/\partial(k_{\rm B}T)$ and spin chiralities $\chi_\gamma(T)=\frac{1}{N}\langle|\sum_i(\boldsymbol{S}_i\times\boldsymbol{S}_{i+\hat{b}})_\gamma|\rangle/S^2$ (γ=a, b, c). Here the brackets denote thermal averages. Concerning the spin chiralities, the $\chi_a(T)$ [$\chi_c(T)$] has a large value, while other two components are nearly zero in the bc-plane [ab-plane] spiral or conical phases. Figure 2(c) shows $C(T)$ and $\chi_\gamma(T)$ at

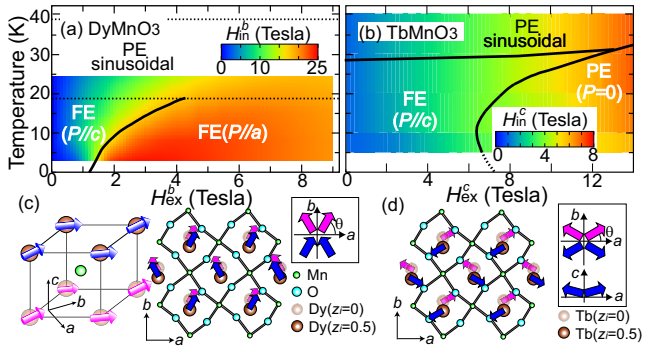

FIG. 3: (color). (a)[(b)] Intensity map of internal magnetic field $H^b_{\rm in}$ [$H^c_{\rm in}$] for $DyMnO_3$ [$TbMnO_3$] in plane of T and external magnetic field $H^b_{\rm ex}$ [$H^c_{\rm ex}$] calculated from experimental magnetization data $m_b(T, H^b_{\rm ex})$ [$m_c(T, H^c_{\rm ex})$], which reproduces the experimental T-$H_{\rm ex}$ diagram in Fig. 1(e)[(f)]. (c)[(d)] Arrangement of the Dy [Tb] f moments in $DyMnO_3$ [$TbMnO_3$] under $\boldsymbol{H}_{\rm ex}\|\boldsymbol{b}$ [$\boldsymbol{H}_{\rm ex}\|\boldsymbol{c}$] where $\theta\sim60^\circ$ [$\theta\sim30^\circ$] [4].

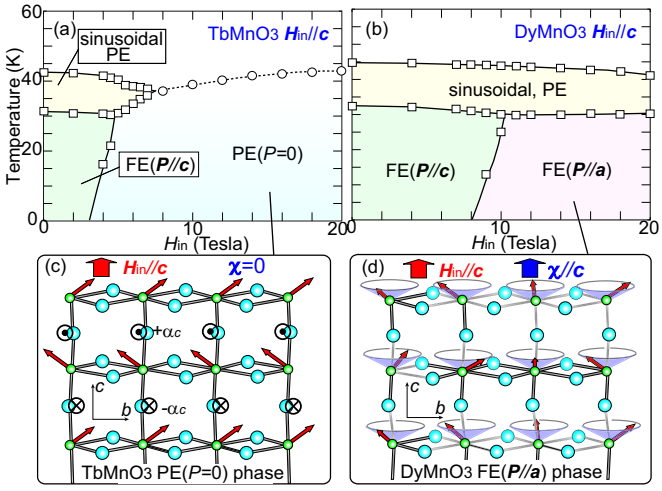

FIG. 4: (color online). Theoretical T-$H_{\rm in}$ phase diagrams of (a) $TbMnO_3$ and (b) $DyMnO_3$ for $\boldsymbol{H}_{\rm in}\|\boldsymbol{c}$, and spin structures in (c) PE(P=0) phase in $TbMnO_3$ and (d) FE($\boldsymbol{P}\|\boldsymbol{a}$) phase in $DyMnO_3$. Dashed line (open circles) in (a) denote the crossover line (points) where $C(T)$ shows a broad maximum.

$H^b_{\rm in}$=8 T for $TbMnO_3$. The $C(T)$ shows three peaks in accord with successive three phase transitions with lowering T. The assignments of spin structures are confirmed by calculating spin and spin-chirality correlations in the momentum space.

By calculating the $H_{\rm in}$ dependence of the expectation value for each term in the Hamiltonian, we identify a mechanism of the chirality flop from $\boldsymbol{\chi}\|\boldsymbol{a}$ to $\boldsymbol{\chi}\|\boldsymbol{c}$ under $\boldsymbol{H}_{\rm ex}\|\boldsymbol{b}$. The bc-plane spiral with $\boldsymbol{\chi}\|\boldsymbol{a}$ at $\boldsymbol{H}_{\rm ex}$=0 is stabilized by the DM interaction associated with the DM vectors on the out-of-plane Mn-O-Mn bonds, i.e., $\mathcal{H}^c_{\rm DM}$. The spins dominantly couple to the a-axis components of the vectors (i.e., components perpendicular to the bc spiral plane) whose signs are the same within a plane but alternate along the c axis, while their magnitudes are all equal to α_c [see Fig. 2(d)]. Without DM interaction, angles between adjacent two spins along the c axis are uniformly ϕ_c=π because of the strong antiferromagnetic (AFM) coupling J_c. In the presence of DM interaction, the angles alternate between $\pi+\Delta\phi_c$ and $\pi-\Delta\phi_c$ with $\Delta\phi_c$>0 [see the inset of Fig. 2(d)]. We can derive a gain of the DM energy due to this angle modulation as $\Delta E^{bc}_{\rm DM}/N = -\alpha_c S^2|\cos\phi_c|\Delta\phi_c$. Without $\boldsymbol{H}_{\rm in}$, the gain $\Delta E^{bc}_{\rm DM}$ in the bc-plane spiral dominates over the easy-(ab)-plane [or the hard-(c)-axis] spin anisotropy from $\mathcal{H}^D_{\rm sia}$, which favors the ab-plane spiral with $\boldsymbol{\chi}\|\boldsymbol{c}$. Note that the value of $|\cos\phi_c|$ is maximum (=1) at $\phi_c=\pi$, but decreases as ϕ_c decreases. This means that the application of $\boldsymbol{H}_{\rm ex}\|\boldsymbol{b}$ suppresses this energy gain since it destroys the interplane AFM coupling and reduces the angle ϕ_c from π. The bc-plane spiral becomes destabilized when the reduced energy gain $\Delta E^{bc}_{\rm DM}$ is defeated by the easy-(ab)-plane anisotropy $\mathcal{H}^D_{\rm sia}$, resulting in the spiral-plane (chirality) flop from bc ($\boldsymbol{\chi}\|\boldsymbol{a}$) to ab ($\boldsymbol{\chi}\|\boldsymbol{c}$). Note that in $R\rm MnO_3$, the ac-plane spiral or conical is unfavorable. This is because it can energetically benefit neither from $\mathcal{H}^D_{\rm sia}$ nor from $\mathcal{H}^c_{\rm DM}$, whereas the ab- and bc-plane spirals can take advantage of one of these two. We expect that the above mechanism is relevant also to the $\boldsymbol{H}_{\rm ex}\|\boldsymbol{b}$ induced $\boldsymbol{P}$ flop from $\boldsymbol{P}\|\boldsymbol{c}$ to $\boldsymbol{P}\|\boldsymbol{a}$ in $LiCu_2O_2$ [6] in terms of the role of $\boldsymbol{H}_{\rm ex}$, which destabilizes the spin spiral with $\boldsymbol{P}\|\boldsymbol{c}$ [14] through destroying the AFM coupling along $\boldsymbol{c}$. Note that the single-ion anisotropy $\mathcal{H}^D_{\rm sia}$ cannot work in this quantum S=1/2 spin system in contrast to $R\rm MnO_3$ with S=2 spins. We expect that the spin spiral with $\boldsymbol{P}\|\boldsymbol{a}$ under $\boldsymbol{H}_{\rm ex}$ (possibly the ab-plane spiral) is stabilized by the other interaction, and the DM coupling with the c-axis components of DM vectors is a possible candidate.

Now we compare our results with experimental ones. Between Figs. 1(e) and Fig. 2(b), there are a few discrepancies. First, threshold fields for the $\boldsymbol{P}$ reorientation are different; i.e., the calculated threshold value of $H^b_{\rm in}$ for $DyMnO_3$ is approximately 18 T, whereas the experimental value of $H^b_{\rm ex}$ is 1-4 T. Second, the slope of the phase boundary is very steep in the theoretical T-$H_{\rm in}$ diagram of Fig. 2(b), while in the experimental T-$H_{\rm ex}$ diagram of Fig. 1(e), it is rather gradual. These discrepancies are solved by considering the effective magnetic field $\boldsymbol{H}_{fd}$ generated by the rare-earth f moments, which acts on the Mn spins via the f-d coupling J_{fd}. Because of the AFM J_{fd}, $\boldsymbol{H}_{fd}$ and $\boldsymbol{H}_{\rm ex}$ are antiparallel, and the internal field $H^\gamma_{\rm in}$ (γ=a, b, c) is given by $H^\gamma_{\rm in}=H^\gamma_{\rm ex}-H^\gamma_{fd}$. Here H^γ_{fd} is written using the f-electron magnetization m_γ as a function of T and $H^\gamma_{\rm ex}$ as $H^\gamma_{fd}(T,H^\gamma_{\rm ex}) = zJ_{fd}m_\gamma(T,H^\gamma_{\rm ex})$. Here z(=8) is the coordination number of R ions around the Mn ion. We assume J_{fd}=0.45 T/$\mu_{\rm B}$ for $DyMnO_3$. Figure 3(a) displays a color plot of the internal magnetic field $H^b_{\rm in}$ in the T-$H^b_{\rm ex}$ plane calculated using the experimental magnetization data. A solid line on which $H^b_{\rm in}$ is

equal to the calculated threshold value is drawn. This figure coincides with the experimental diagram of $DyMnO_3$ in Fig. 1(e). A similar analysis for $TbMnO_3$ has also reproduced the experimental diagram (not shown). The roles of the f-d coupling in RMnO$_3$ at $H_{\rm ex}$=0 have been studied by recent neutron-scattering experiments [15, 16]. We find that the switching of $\boldsymbol{P}$ can be qualitatively understood even without considering the f-d coupling, but it should be taken into account for quantitative discussion.

Next we discuss the case of $\boldsymbol{H}_{\rm ex}\|\boldsymbol{c}$. The theoretical T-$H^c_{\rm in}$ phase diagrams of $TbMnO_3$ and $DyMnO_3$ are displayed in Figs. 4(a) and (b). In Fig. 4(a), we find the transition to a coplanar spin state with $\boldsymbol{P}$=0 for $TbMnO_3$ at $H^c_{\rm in}\sim$3-5 T, which coincides with the experimental observation of paraelectric phase under $\boldsymbol{H}_{\rm ex}\|\boldsymbol{c}$. For its magnetic structure, see Fig. 4(c). Again, there are a few discrepancies between the theoretical and experimental results [compare Figs. 1(f) and Fig. 4(a)]. They are resolved by considering the influence of Tb f moments. In Fig. 3(b), we display the T and $H^c_{\rm ex}$ dependence of the internal field $H^c_{\rm in}$ calculated from the experimental magnetization data. Here we assume J_{fd}=0.65 T/$\mu_{\rm B}$ for $TbMnO_3$. Solid lines on which $H^c_{\rm in}$ is equal to the calculated threshold value are drawn. This figure coincides well with the experimental diagram of $TbMnO_3$ in Fig. 1(f). On the other hand, the transition to the ab-plane transverse conical state with $\boldsymbol{P}\|\boldsymbol{a}$ [see Fig. 4(d)] is found for $DyMnO_3$ in Fig. 4(b), which has not been observed in experiments up to $H^c_{\rm ex}$=9 T. The required $H^c_{\rm ex}$ for this transition deviates from the calculated critical value of $H^c_{\rm in}$ by the field $\boldsymbol{H}_{fd}$ from the Dy f moments antiparallel to $\boldsymbol{H}_{\rm ex}$. Hopefully, the reorientation of $\boldsymbol{P}$ will be observed in $DyMnO_3$ under a higher $H^c_{\rm ex}$.

The contrasting behaviors of $\boldsymbol{P}$ under $\boldsymbol{H}_{\rm ex}\|\boldsymbol{c}$ between $DyMnO_3$ and $TbMnO_3$ can be attributed to the difference in magnitude of the in-plane spin-exchange J_b. $TbMnO_3$ has much smaller J_b=0.64 meV than $DyMnO_3$ with J_b=0.99 meV. At $H_{\rm ex}$=0, the Mn spins form a spiral order to minimize the spin-exchange energy in both compounds. Once we apply $\boldsymbol{H}_{\rm ex}\|\boldsymbol{c}$, the ferromagnetic moment is induced along the c axis, and hence rotating components of the spins become reduced. Then in $TbMnO_3$ with a small J_b, the spiral and conical spin orders no longer take advantage of the spin exchanges under $\boldsymbol{H}_{\rm ex}\|\boldsymbol{c}$, resulting in the first-order transition to the coplanar state as shown in Fig. 4(c). This state can benefit from all of the large a-axis components of the DM vectors on the out-of-plane bonds, which are perpendicular to the coplanar spin plane. The $\boldsymbol{H}_{\rm ex}$-induced ferroelectric-to-paraelectric transition with sudden vanishing of $\boldsymbol{P}$ has also been observed in many other spin-spiral multiferroics, e.g., $Ni_3V_2O_8$ [8] and $MnWO_4$ [7]. We expect that the above mechanism is relevant also to them.

In summary, we have theoretically studied the puzzling T-$H_{\rm ex}$ phase diagrams of the spin-spiral multiferroic RMnO$_3$ (R=Tb and Dy) and have revealed new mechanisms for the magnetic control of $\boldsymbol{P}$ by analyzing a microscopic spin model using the MC technique. We have shown that the applied $\boldsymbol{H}_{\rm ex}\|\boldsymbol{Q}$ ($\|\boldsymbol{b}$ in the present case) reduces the DM energy through modulating the interplane spin angles, and thereby controls a competition between $\mathcal{H}^c_{\rm DM}$ and other interaction ($\mathcal{H}^D_{\rm sia}$ in the present case), which results in the spiral-plane or spin-chirality flop with reorientation of $\boldsymbol{P}$. On the other hand, the applied $\boldsymbol{H}_{\rm ex}\perp\boldsymbol{Q}$ ($\|\boldsymbol{c}$ in the present case) suppresses the spin-exchange energy through reducing the rotating components of spins, and thereby causes a competition between the spin exchanges $\mathcal{H}_{\rm ex}$ and other interaction ($\mathcal{H}^c_{\rm DM}$ in the present case). As a result, the first-order transition from spiral to coplanar spin phases occurs in $TbMnO_3$ with a rather small J_b accompanied by the sudden disappearance of $\boldsymbol{P}$. We have discussed that the proposed mechanisms are also applicable to many other spin-spiral multiferroics. Additionally, we have found that the experimental results can be quantitatively reproduced by considering the effective field $\boldsymbol{H}_{fd}$ from the rare-earth f moments.

We thank Y. Tokura and N. Nagaosa for valuable discussions. MM thanks H. Murakawa and Y. Tokunaga for their experimental supports. This work was supported by Grant-in-Aid (No.22740214) and G-COE Program ("Physical Sciences Frontier") from MEXT Japan, and Funding Program for World-Leading Innovative R&D on Science and Technology (FIRST Program) from JSPS.

[1] T. Kimura *et al.*, Nature (London) **426**, 55 (2003).
[2] Y. Tokura, J. Magn. Magn. Mater. **310**, 1145 (2007); S.-W. Cheong and M. Mostovoy, Nat. Mater. **6**, 13 (2007).
[3] T. Kimura, Annu. Rev. Mater. Res. **37**, 387 (2007).
[4] T. Kimura, G. Lawes, T. Goto, Y. Tokura, and A. P. Ramirez, Phys. Rev. B **71**, 224425 (2005).
[5] H. Murakawa *et al.*, Phys. Rev. Lett. **101**, 197207 (2008).
[6] S. Park, Y. J. Choi, C. L. Zhang, and S.-W. Cheong, Phys. Rev. Lett. **98**, 057601 (2007).
[7] K. Taniguchi *et al.*, Phys. Rev. B **77**, 064408 (2008).
[8] M. Kenzelmann *et al.*, Phys. Rev. B **74**, 014429 (2006).
[9] M. Mostovoy, Phys. Rev. Lett. **96**, 067601 (2006).
[10] H. Katsura, N. Nagaosa, and A. V. Balatsky, Phys. Rev. Lett. **95**, 057205 (2005).
[11] M. Kenzelmann *et al.*, Phys. Rev. Lett. **95**, 087206 (2005).
[12] N. Aliouane *et al.*, Phys. Rev. Lett. **102**, 207205 (2009).
[13] Y. Yamasaki *et al.*, Phys. Rev. Lett. **101**, 097204 (2008).
[14] Y. Kobayashi *et al.*, J. Phys. Soc. Jpn. **78**, 084721 (2009).
[15] O. Prokhnenko *et al.*, Phys. Rev. Lett. **98**, 057206 (2007).
[16] O. Prokhnenko *et al.*, Phys. Rev. Lett. **99**, 177206 (2007).
[17] For their direction vectors, we use the structural data of $TbMnO_3$ and $DyMnO_3$; see J. A. Alonso, M. J. Martínez-Lope, M. T. Casais, and M. T. Fernández-Díaz, Inorg. Chem. **39**, 917 (2000).
[18] I. Solovyev, N. Hamada, and K. Terakura, Phys. Rev.

Lett. **76**, 4825 (1996).
[19] M. Mochizuki, and N. Furukawa, Phys. Rev. B **80**, 134416 (2009).
[20] K. Hukushima and K. Nemoto, J. Phys. Soc. Jpn. **65**, 1604 (1996).